



Mechanics Based Design of Structures and Machines

An International Journal

ISSN: (Print) (Online) Journal homepage: <https://www.tandfonline.com/loi/lmbd20>

Design of biaxial flexural mount for a rectangular mirror with large aspect ratio of a space telescope

Ruijing Liu, Zongxuan Li, Xiubin Yang, Qingya Li & Qiang Yong

To cite this article: Ruijing Liu, Zongxuan Li, Xiubin Yang, Qingya Li & Qiang Yong (2021): Design of biaxial flexural mount for a rectangular mirror with large aspect ratio of a space telescope, Mechanics Based Design of Structures and Machines, DOI: [10.1080/15397734.2021.1922287](https://doi.org/10.1080/15397734.2021.1922287)

To link to this article: <https://doi.org/10.1080/15397734.2021.1922287>



Published online: 10 May 2021.



Submit your article to this journal [↗](#)



Article views: 18



View related articles [↗](#)



View Crossmark data [↗](#)



Design of biaxial flexural mount for a rectangular mirror with large aspect ratio of a space telescope

Ruijing Liu^{a,b,c}, Zongxuan Li^{a,c} , Xiubin Yang^{a,c}, Qingya Li^{a,c}, and Qiang Yong^{a,c}

^aChangchun Institute of Optics, Fine Mechanics and Physics, Chinese Academy of Sciences, Changchun, Jilin, China; ^bUniversity of Chinese Academy of Sciences, Beijing, China; ^cKey Laboratory of Space-based Dynamic & rapid Optical Imaging technology, Chinese Academy of Sciences, Changchun, Jilin, China

ABSTRACT

In this paper, the biaxial flexural mount is presented according to the requirements of the large aspect ratio mirror of an off-axis three-mirror anastigmatic (TMA) space-borne telescope, and the process of the optimal design of the flexural mount structure is discussed in detail. From the perspective of mechanics-based design of space-borne mirror assembly structure and integrated optical-mechanical analysis, the optimal axial mounting position, the optimal mounting angle and the optimal structural critical dimensions of the flexure hinge were determined to improve the surface shape accuracy. Finally, the mechanical vibration test further proved the rationality of the structure design and the accuracy of the simulation analysis. The flexural mount proposed in this paper is can be applied to other reflective optics with high surface figure requirements. The optimization method proposed in this paper can also be applied to the optimization of other forms of flexural mount.

ARTICLE HISTORY

Received 29 October 2020
Accepted 23 April 2021

KEYWORDS

Rectangular mirror; flexural mount; optical-mechanical integration analysis; space telescope

1. Introduction

Compared with the coaxial system, the off-axis three-mirror anastigmatic (TMA) optical system has no central obscuration, high MTF, and can obtain high-quality remote sensing images. There are more than 10 TMA space optical cameras on orbit all over the world since 1990s. Rectangular reflective mirrors are the critical imaging components of large aperture spaced-borne or ground-based telescopes. The tertiary mirror of Quickbird-2 of the United States is in the form of rectangular shape. The conic tertiary mirror has a surface figure error of 0.009λ RMS over its entire $1820 \text{ mm} \times 668 \text{ mm}$ surface (Figoski 1999). The size of primary mirror for PRISM-2's telescope on JAXA's ALOS satellite is near $900 \text{ mm} \times 600 \text{ mm}$ (Suzuki et al. 2012). The accuracy of the mirror surface figure directly affects the imaging quality of the optical system. Space telescope experience harsh environments such as vibration, shock, and gravity release during fabrication, testing, mounting, transportation, launching, and on orbit. It is necessary to ensure that the mirror assembly maintains a good surface accuracy after those loads.

The surface figure accuracy of the large aspect ratio mirror of a space telescope is guaranteed by the stiffness of the mirror and the environmental adaptability of the mounted structure. In order to ensure the good adaptability of the reflector to the environment, the concept of flexible hinge is proposed. Flexible hinges are widely used in various fields, such as flexural mount for mirror, flexible manipulator, flexible spine, etc (Bhattacharya, Anantha Suresh, and Ghosal 2018;

Omid, Fathollahi, and Habibnejad 2020; Riabtsev et al. 2020). While ensuring the stiffness and strength of the mirror body, it must ensure that the flexible hinge of the flexural mount does not fail in the launching environment. Once the hinge fails, it will directly cause the mirror to deviate from the aligned position, enabling the optical system to image. More than that, the flexure mount should have lateral flexibility to minimize the stress in the optics and enough axial rigidity to support the mirror effectively (Doyle, Genberg, and Michels 2012). Many scholars have researched on the flexural mount for large-aperture space mirrors. B. Liu et al. proposed an adjustable bipod flexure for circular mirrors, which can effectively reduce the aberration caused by gravity in the optical axis by adjusting the distance between the two legs, the surface RMS value is 8.1 nm (Liu et al. 2018). H. Kihm proposed a new bipod flexure for a mirror with a diameter of 800 mm. It can compensate the surface figure error and assembly error under the action of gravity by adjusting the thickness of gaskets on the flexure mount the surface RMS value is 7.5 nm (Kihm et al. 2012). Z. X. Li et al. proposes a Cartwheel biaxial flexural hinge for $\phi 750$ mm primary mirror, the mirror surface error is 9 nm RMS (Li, Chen, and Jin 2018). Z. Zhang et al. of Tsinghua University designed a low stress flexural mounting structure, which can ensure the surface figure accuracy of the mirror by finding the most suitable bolt pre-tightening force (Zhang et al. 2017). H. X. Li et al. designed a two-axis flexure structure for a 760 mm \times 320 mm mirror, with the RMS value is 13.4 nm and the first-order natural frequency of 128.67 Hz under gravity (Li, Ding, and Zhang 2015). Z. X. Li et al. propose a cartwheel flexural mount for a $\phi 760$ mm SIC mirror, with the RMS value is better than $\lambda/50$ (Li et al. 2017).

Sharma et al analyzed the structural static response of the curved composite structure by means of isoparametric finite element steps in association with Reddy's higher order mid-plane theory, and predicted the optimal deflection and stacking sequence. Arijit et al used high-order finite element and soft computing techniques to derive a hybrid coupling technique to predict the optimal stacking sequence of the layered structure and the corresponding frequency values (Arijit et al. 2018). Lalepalli et al. also adopted a hybrid finite element method to predict the best fiber volume fractions and the minimal mass of the layered composite structure (Lalepalli et al. 2020).

The aperture of the rectangular mirror of an off-axis three-mirror anastigmatic (TMA) telescopes is 1340 mm \times 150 mm. The slim light-weighted space-borne mirror has a very large aspect ratio (larger than the reported rectangular mirrors that can be found in literatures, such as Quickbird-2), and has critical requirements on the surface figure accuracy and the first-order natural frequency of the mirror assembly structures. A novel flexural mount is designed for the mounting and gravity offloading requirements of the mirror. As shown in Figure 1, different from the traditional flexible hinge design of mirror mount, the rotation centers of the upper and lower flexible hinges of the flexible hinge are not on the same plane, which can provide better translational freedom. Compared with the traditional flexure hinge, it can better offload the mirror body deformation caused by the external force load and the assembly error. The surface shape accuracy of the mirror body. The two-axis orthogonal flexural mount structure is adopted, which can not only ensure sufficient structural support rigidity, but also meet the stress adjustment requirements.

The integrated optical-mechanical analysis method is used to explore the influence of flexural mount on the surface accuracy of Wave Front Error (WFE, which is quite critical for optical imaging systems) of the mirror. By optimizing the axial mounting position and mounting angle, the surface figure accuracy is guaranteed. Then we proposed to further improve the surface figure accuracy by finding the critical dimensions of the flexure hinge. We established a flexure hinge model and optimize the three critical dimensions of the flexure hinge at the same time to obtain the optimal dimension parameters to ensure the surface figure accuracy. Finally, the relationship between the three critical dimensions of the flexure hinge and the surface accuracy and the first-order natural frequency is investigated in a Four Dimension Space form. The delicate designed

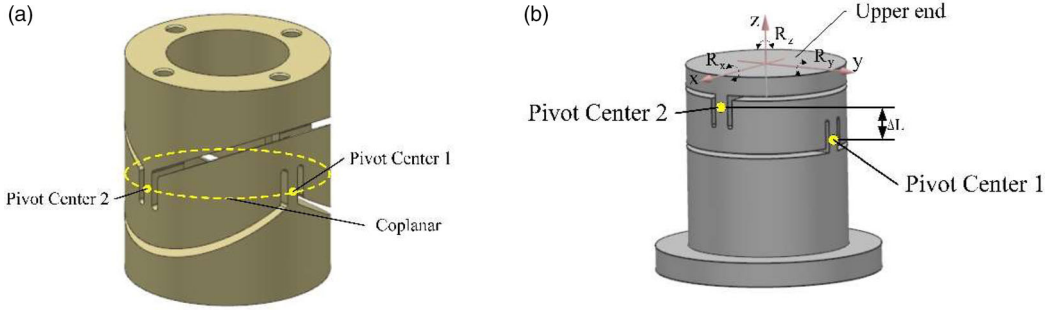


Figure 1. Flexure Mount (a) the traditionally used coplanar biaxial flexures, (b) the Non-coplanar biaxial flexures.

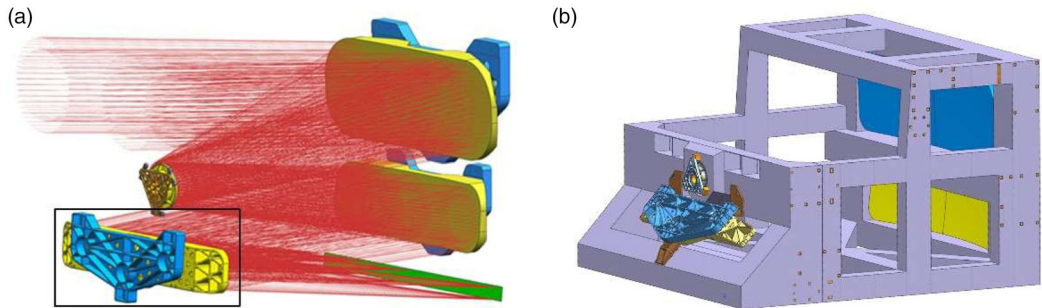


Figure 2. The rectangular mirror of an off-axis TMA telescope (a) the optical system of the TMA telescope, (b) the structure of the TMA telescope.

flexural mount proposed in this paper can meet the requirements, the x/y surface figure accuracy of the mirror under the action of 1 G gravity is 4.97 nm/2.91 nm respectively (far below the required 10 nm RMS), and the fundamental frequency is 228.27 Hz (higher than 200 Hz to avoid resonance by launch loads). Finally, an aluminum prototype was developed, the vibration test was carried out, and the results of simulation analysis were compared to verify the rationality and accuracy of the flexural mount design.

2. Design of mirror and flexural mount

The mirror assembly is composed of a mirror and its mounting structure. The surface figure accuracy of the mirror directly affects the imaging quality of the optical system. The size and weight of the mirror also affect the overall structure and weight of the optical system. It is necessary to design the structure of the mirror assembly according to the requirements of the optical system for the mirror.

2.1. Lightweight design of SiC mirror

In order to ensure the surface accuracy of the mirror, the mirror material must have the characteristics of physical structure stability, high stiffness and good thermal stability. Taking the circular mirror as an example, without considering its transverse shear effect, the natural frequency f_n and the gravitational deformation δ are respectively (Doyle, Genberg, and Michels 2012)

$$f_n = \frac{C}{r^2} \sqrt{\frac{E}{\rho}} \sqrt{\frac{T}{12(1-\mu^2)}} \quad (1)$$

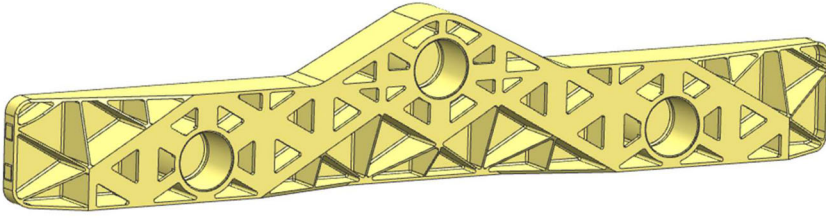


Figure 3. The lightweight structure of the mirror.

$$\delta = C \left(\frac{r^4}{T^4} \right) \left(\frac{\rho}{E} \right) (1 - \mu^2) \quad (2)$$

where E is the elastic modulus of the material, ρ is the material density, r is the mirror radius, C is the constant related to the mirror material, T is the mirror thickness, μ is the material poisson's ratio, E/ρ is the specific stiffness. It can be seen from formula (1) (2) that the greater the specific stiffness of the material, the greater the natural frequency f_n , and the smaller the self-weight deformation value δ , the stronger the deformation resistance under complex working conditions, and the easier it is to maintain high surface figure accuracy. RB-SiC self-developed by the Changchun Institute of Optics, Fine Mechanics of the Chinese Academy of Sciences (CIOMP) was selected as the mirror material.

In order to avoid the redundant mass of the mirror and reduce the launch cost, a lightweight design of the mirror is required. The most common lightweight patterns are triangle, quadrilateral and hexagon, and the triangle has the highest specific stiffness (Guo et al. 2019). Therefore, triangular pattern is chosen to lightweight the rectangular mirror. As for the selection of the closed form of the back, the semi-closed structure is adopted on the back of the mirror after comprehensive consideration of the technology and the rigidity of the mirror.

The stiffness of the mirror is not sensitive to the thickness of the ribs. On the premise of ensuring the stiffness of the mirror body, the thickness of the reinforcement is designed as thin as possible (Zhang et al. 2017). For the feasibility of manufacturing, the rib thickness is designed to be 3 mm.

Back mounting usually utilize three points, six points, or nine points. The number of support points can be estimated by formula (3)

$$N = \frac{1.5r^2}{T} \sqrt{\frac{\rho g}{E\delta}} \quad (3)$$

where E is the elastic modulus of the material, ρ is the material density, r is the mirror radius, T is the mirror thickness, g is the acceleration of gravity; δ is the maximum self-gravity deformation, $N \approx 3$ can meet the requirement of maximum deformation (Wang 2019). Therefore, the mounted scheme is determined as the most classic three-point mount method. For the mirror mounted by three points on the back, the triangle centroid formed by the three mount points should coincide with the centroid of the mirror body, to avoid generating additional torque (Doyle, Genberg, and Michels 2012). The lightweight structure of the mirror is shown in Figure 3, and the main structural parameters are shown in Table 1.

2.2. Design of flexural mount

The flexural mount is needed to offload gravity and thermal stress, to make the mirror surface figure insensitive to environmental change. Flexural mount is an important part of the mirror assembly. It can isolate vibration and mounting stress propagation, but also absorb the local strain caused by the mismatch of the thermal expansion coefficient of the material under



Figure 4. Machined test piece of the flexural mount.

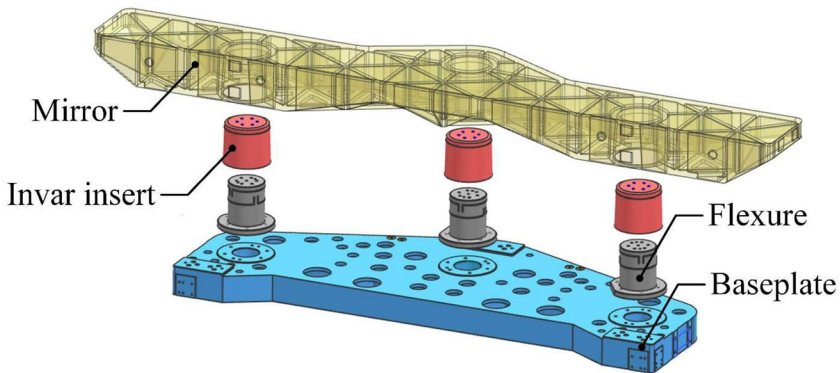


Figure 5. The mirror assembly structure design.

Table 1. Mirror structure parameters.

Item	Value/mm
Total height	88
Front surface thickness	5
Back surface thickness	7
Core rib thickness	3
Rib spacing interval	96.5
Mount hole diameter	106

temperature changes. Therefore, the flexural mount should not only have good mount stiffness and play an important role in positioning the mirror, but also have compliance to unload the thermal stress of the mirror.

In order to realize the mounting and positioning of RB-SiC mirror with flexural mount, the mirror needs to provide mechanical interface and support structure for screw connection and pin positioning. Considering the mechanical connection performance of the insert and the matching with the linear expansion coefficient of the mirror, the insert material used is a low-expansion alloy of grade 4J36. Titanium alloy (TC4) is selected as the flexural mount material connected

Table 2. material properties of the mirror assembly.

Material	Density/(kg/mm ³)	Young's modulus/ Mpa	Thermal conductivity/(W*m ⁻¹ *K ⁻¹)	Coefficient of thermal expansion/(10 ⁻⁶ *K ⁻¹)	Poisson's ratio
RB-SiC	3.05E-9	330000	185	2.5	0.33
4J36	8.10E-9	141000	13.9	2.3	0.25
TC4	4.44E-9	109000	8.8	9.1	0.34
SiC/Al	2.94E-9	180000	225	8.1	0.18

with the metal inserts, which has the advantages of low density, high specific stiffness, excellent stability, and good mechanical processing, etc. For the substrate materials connected with the flexural mount, silicon carbide particulate reinforced Al-matrix composite(SiC/Al) is selected, which has the advantages of high specific stiffness, low linear expansion coefficient and high thermal conductivity, etc. The material properties of the mirror assembly are shown in Table 2.

After the material of the mirror assembly is determined, the structure design and finite element simulation analysis of the biaxial flexure hinge are carried out according to the mount requirements of the mirror. The mirror has three degrees of freedom of movement $T_x/T_y/T_z$ and three degrees of freedom of rotation $R_x/R_y/R_z$. The flexural mount needs to constrain these six degrees of freedom. It is planned to design a biaxial flexible hinge, which has two orthogonal flexible grooves machined on a cylinder with an outer diameter of r , so that the upper end of the flexural mount has five directions of $R_x/R_y/R_z/T_x/T_y$ flexible deformation freedom.

The flexure hinge can be set as a short beam blade with small mounting angular stroke and high position accuracy. The design of the flexure hinge is a hollow cylinder with flange mounting surface. Figure 4 is machined piece of the designed biaxial straight beam blade flexure hinge. An L-shaped flexible groove is cut in the orthogonal direction of the cylinder with a radius of r to provide rotational freedom and translation freedom around the x/y direction respectively. Figure 5 is the configuration of the mirror mounting system, including three flexures, three Invar inserts, and one baseplate.

3. Optimal design of flexure mounting

In order to ensure that the mirror has good surface figure accuracy under external loads, integrated opto-mechanical analysis is performed on the mirror assembly. The structure of the mirror body is very complicated. Only by repeatedly optimizing the mirror structure will not only increase the manufacturing cost, but even cannot be manufactured due to processing technology. Optimizing the flexural mount is the most reasonable and simple way. After the optimization analysis of the mirror structure, optimizing the flexural mount structure on this basis can further improve the accuracy of the mirror surface. Moreover, as the weakest part in the mirror assembly, the flexible hinge needs to have a certain support rigidity to play a role of positioning mount. Once damaged, the entire optical system cannot be imaged. A certain degree of flexibility is also required to allow the flexible hinge to have a certain amount of deformation, which can offload the external load and ensure the surface accuracy. Therefore, it is necessary to repeatedly optimize the flexible support structure. Next, the optimization analysis will be carried out from the three aspects of the flexural mount axial mounting position, the mounting angle, and the critical dimensions of the flexible hinge.

3.1. Optimization of axial mounting and positioning

When the optical axis is placed horizontally, the elastic micro-deformation of mirror is generated under gravity. The deformation can be offloaded by the flexural mount to minimize the wave

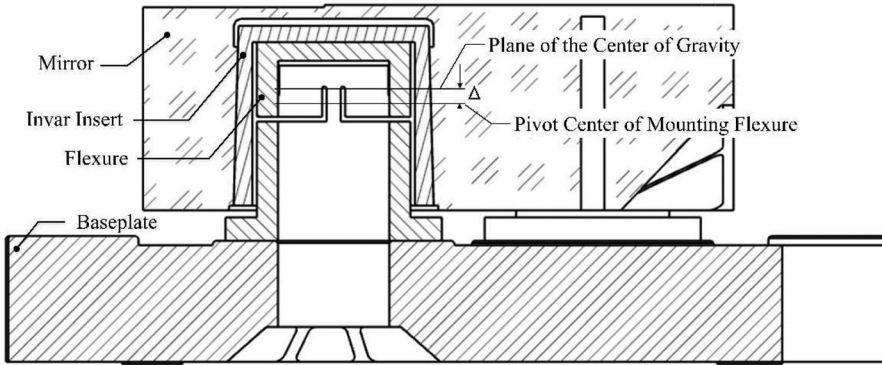


Figure 6. The position relationship between the pivot center of mounting flexure and the mirror gravity center.

front error (WFE) of mirror. Designate the distance Δ between the plane formed by the three mounting points and the center of gravity of the mirror, the gravity of the mirror is G , and the moment generated by its own weight can be expressed by formula (4)

$$M = G\Delta \quad (4)$$

When the plane formed by the three mounting points coincides with the center of gravity of the mirror, that is $\Delta=0$, the resultant moment generated by the self-weight deformation of the mirror is zero.

Figure 6 is a schematic diagram of the position relationship between the pivot center of mounting flexure and the mirror gravity center. The distance between the two surfaces is Δ . The Δ is negative when the pivot center of mounting flexure is below the center of gravity of the mirror, and the value is positive when the pivot center of mounting flexure is above the center of gravity of the mirror. During the polishing and testing of the mirror assembly on the ground, there will be gravitational deformation in the x/y direction, especially in the y direction, so the flexural mount must be able to unfold the x/y gravity load well.

The finite element model of the PMA is built using commercial FEA pre-processing software MSC/PATRAN, as shown in **Figure 7**. Totally 338,275 elements comprise the analysis model. All the three DOFs of nodes on the three mounting surface of the baseplate are fixed as boundary conditions. Lateral gravity, and axial gravity change are applied to the FEM model, respectively, to perform the static analysis so as modal analysis. The analysis results are shown in **Figures 8** and **9** respectively.

Based on the analysis above, we can conclude that the surface error of the mirror under lateral gravity is barely influenced by Δ . There is a sweet point in **Figure 8**. When $\Delta=0$, the x/y surface shape accuracy is $RMS_x=5.96$ nm and $RMS_y=3.52$ nm respectively, indicating that the mirror surface distortion generates almost no high order aberration terms. Thus, we infer that the distance Δ must be zero if the surface error under lateral gravity is required for a minimum control. From **Figure 9**, when $\Delta=0$, the fundamental frequency of the mirror component is 195.94 Hz. **Figure 10** shows the modal shapes of the first 6 modes, and **Figure 11** shows the residual surface error of the mirror under 1G lateral gravity. The rigid-body-motion and power in Zernike polynomial fitting is removed.

3.2. Optimization of mounting angle

When the flexural mount is assembled with other components, the mounting angle between it and the assembly datum plane will affect the mirror shape accuracy. This paper proposed to

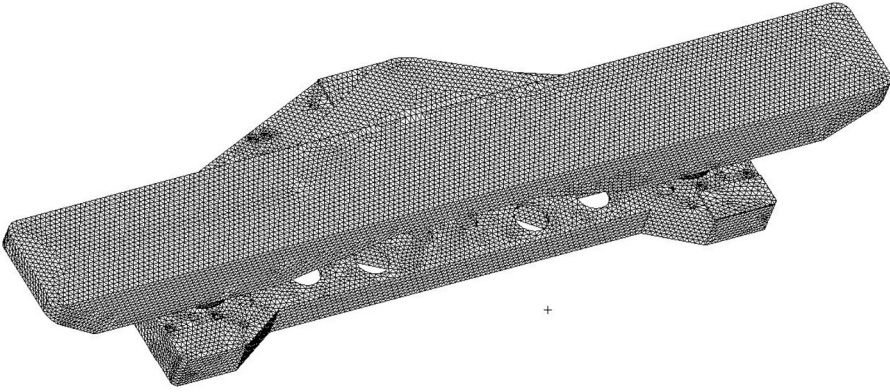


Figure 7. The finite element model of the mirror.

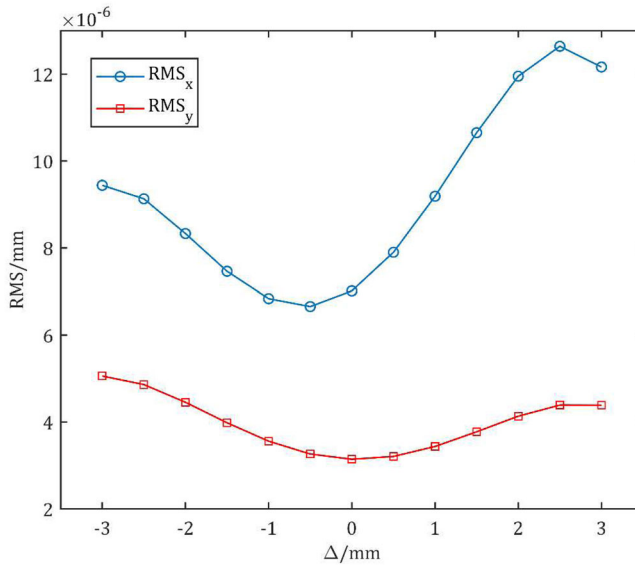


Figure 8. Mirror surface distortion due to Δ under 1G lateral gravity.

further improve the surface figure accuracy by finding the optimal mounting angle of the flexural mount on the basis of obtaining the optimal axial mounting position of the flexural mount.

As shown in [Figure 12](#), the substrate has a symmetrical structure on both sides, the optical axis direction is set to the z axis direction, the short side direction is marked as y axis, the long side direction is marked as x axis, the symmetry plane yoz is the reference plane. A respective reference coordinate system is established at the center of the upper end surface of each flexural mount. The plane of the center of the rotation axis of each flexural mount is $y_1o_1z_1/y_2o_2z_2/y_3o_3z_3$, and the included angle of the yoz surface is recorded as $\alpha_1/\alpha_2/\alpha_3$.

The biaxial flexural mount is a rotationally symmetric structure, and the flexural mount 1 is located exactly on the symmetry plane yoz , and its mounting angle $\alpha_1=0^\circ/90^\circ$. In order to determine the optimal mounting angle, first set $\alpha_1=0^\circ$, and then keep the flexural mount 1 still, and the flexural mount 2/3 rotate relative around its rotation axis at the same time, and then use the large-step optimization method to determine the optimal mounting angle interval. Change the parameters of α_2/α_3 within the interval, and perform static analysis on the mirror assembly, and

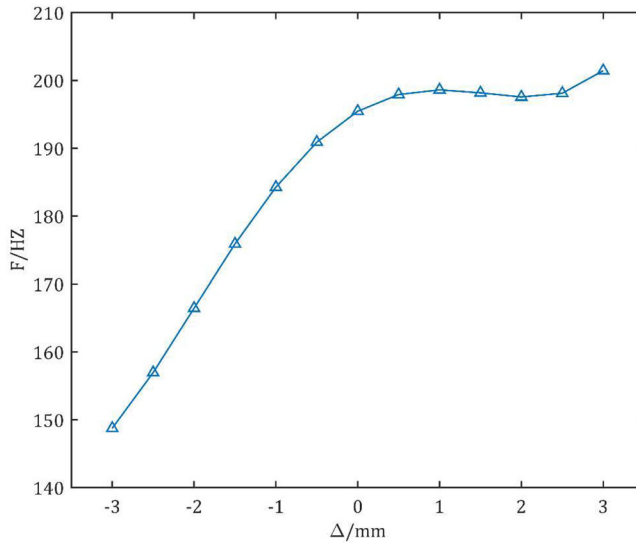


Figure 9. The fundamental frequency of the mirror assembly due to Δ .

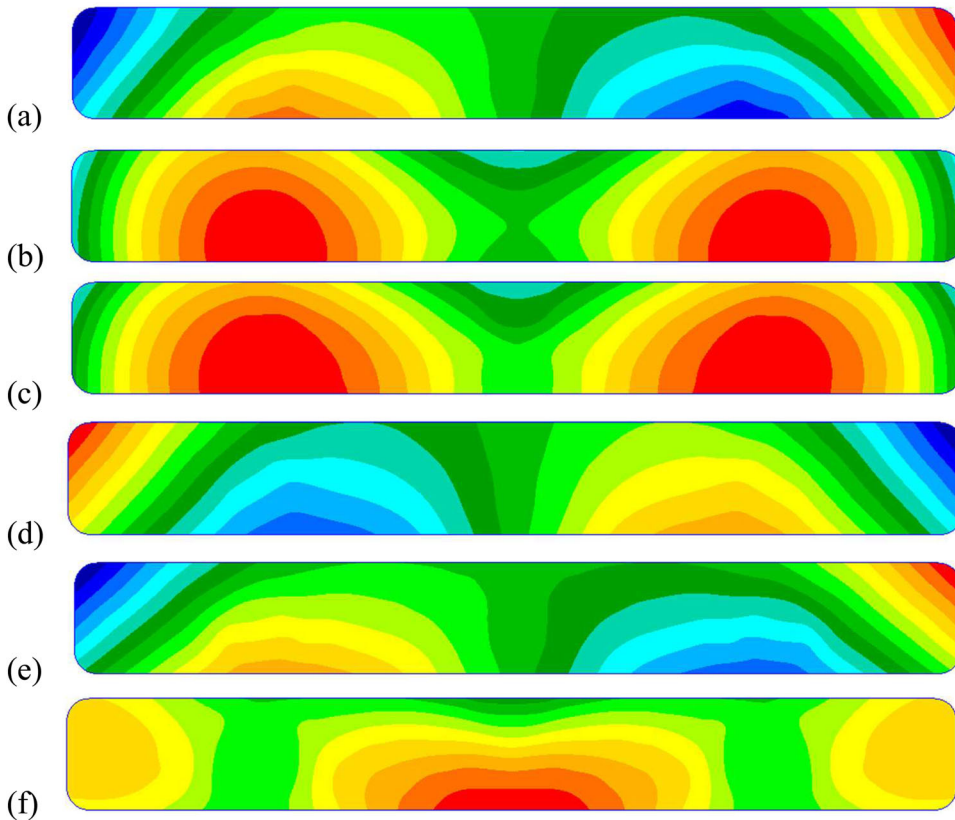


Figure 10 The modal shapes of the first 6 mode (a) $F_1 = 195.94$ Hz, (b) $F_2 = 199.79$ Hz, (c) $F_3 = 228.23$ Hz, (d) $F_4 = 238.81$ Hz, (e) $F_5 = 241.73$ Hz, (f) $F_6 = 260.15$ Hz.

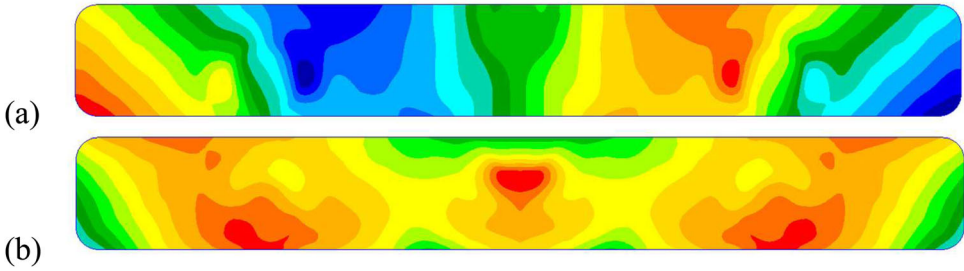


Figure 11. The deformation fringe of static analysis results, (a) surface distortion due to x-direction gravity, $RMS_x=5.96$ nm, (b) surface distortion due to y-direction gravity, $RMS_y=3.52$ nm.

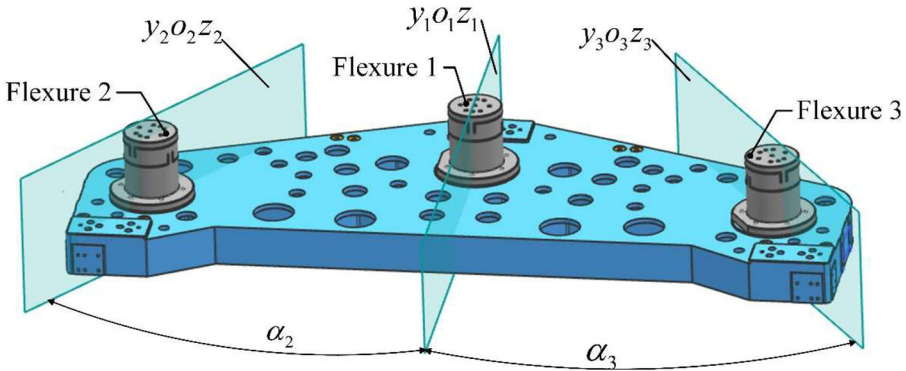


Figure 12. Mounting angle of flexural mount.

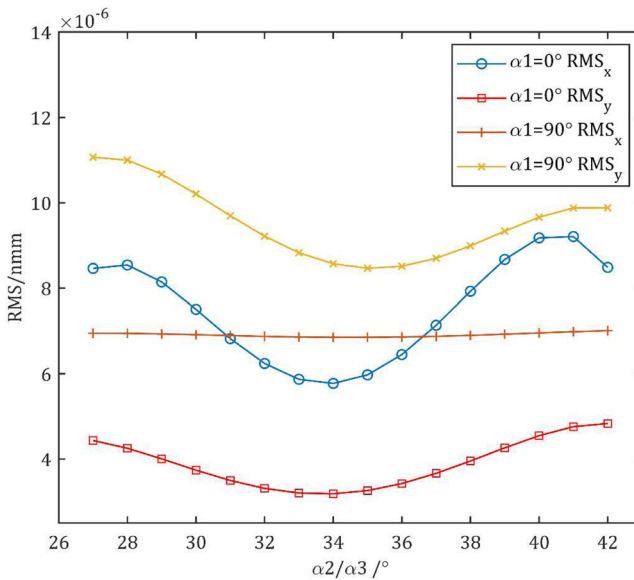


Figure 13. Mirror surface distortion due to mounting angle under 1G lateral gravity.

obtain the influence of α_2/α_3 on the surface accuracy of the mirror surface and the first-order frequency of the mirror assembly under the action of 1G on the optical axis horizontally. Let $\alpha_1=90^\circ$, and repeat the above optimization steps. The final analysis result is shown in Figure 13.

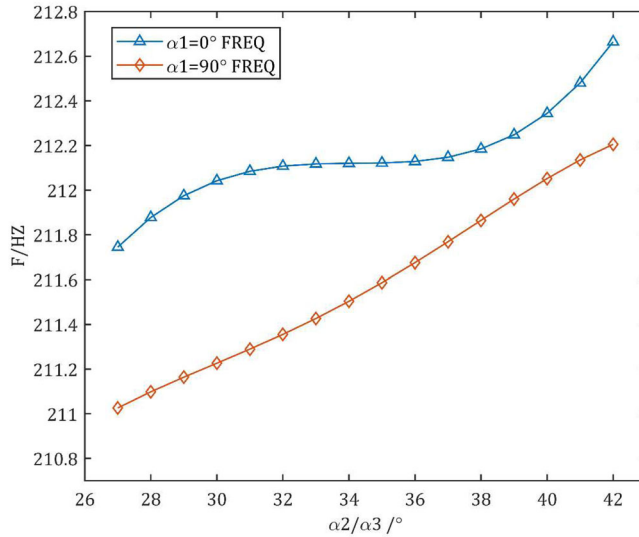


Figure 14. The fundamental frequency of the mirror assembly due to mounting angle.

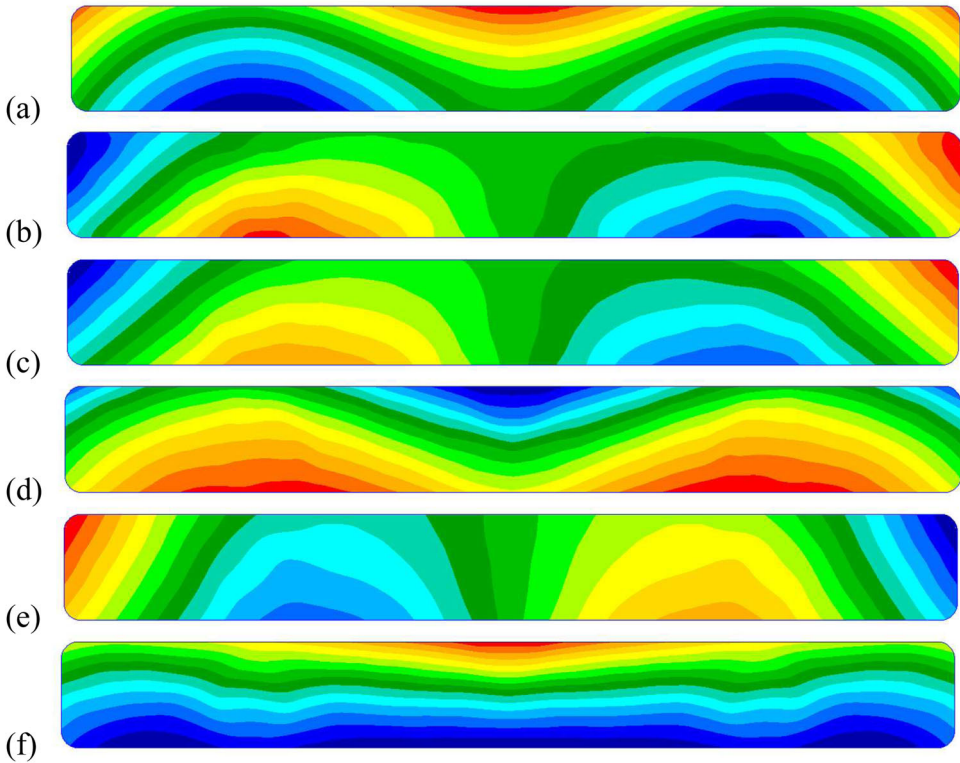


Figure 15. The modal shapes of the first 6 modes, (a) $F_1 = 212.08$ Hz, (b) $F_2 = 212.2$ Hz, (c) $F_3 = 236.91$ Hz, (d) $F_4 = 245.52$ Hz, (e) $F_5 = 250.30$ Hz, (f) $F_6 = 271.85$ Hz.

It can be seen from Figure 13 that the accuracy of the reflection mirror shape varies with the angle between the middle flexural mount 1 and the middle flexural mount 2/3. The simulation analysis results in Figure 13 show that the surface accuracy of the x/y direction is poor when the

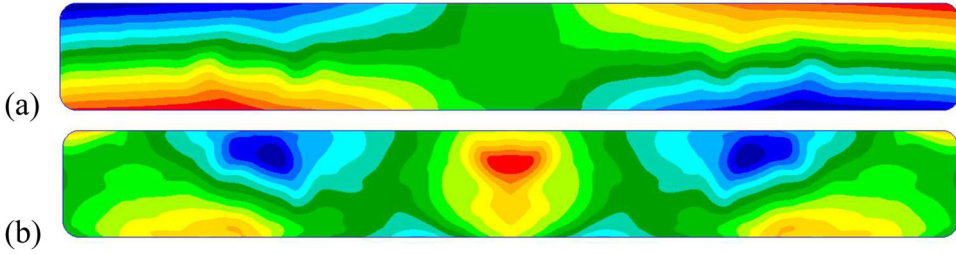


Figure 16. The deformation fringe of static analysis results, (a) surface distortion due to x-direction gravity, $RMS_x=5.72$ nm, (b) surface distortion due to y-direction gravity, $RMS_y=3.01$ nm.

mounting angle is $\alpha_1=90^\circ$. When $\alpha_1=0^\circ$ and α_2/α_3 are $-34^\circ/34^\circ$, the surface error of the mirror is minimized only with $RMS_x=5.72$ nm, $RMS_y=3.01$ nm. From Figure 14, we can see the fundamental frequency slightly inclined with respect to mounting angle. Figures 15 and 16, respectively shows the modal shapes of the first 6 modes of the mirror module after removing the rigid body displacement and the mirror surface error under the action of 1 G gravity.

The precise positioning and mounting angle of the flexural mount along the optical axis can not only accurately position the mirror body in the axial direction, but also improve the accuracy of the mirror surface. Before adjusting the mounting angle, the fundamental frequency of the mirror assembly is 195.94 HZ, and after adjustment, the fundamental frequency reaches 212.08 HZ. Adjusting the mounting angle can improve the overall static and dynamic stiffness of the component, which is of great significance for maintaining the surface accuracy of the mirror under various working conditions.

3.3. Optimization of flexure hinge structure parameters

After determining the axial mounting position and mounting angle of the flexural mount, the critical dimensions of the flexural mount can be optimized in order to find the best surface accuracy of the mirror surface and the reliability of the structure. Flexural mount not only needs to produce certain deformation to achieve the purpose of offloading load, but also has a certain stiffness to play the role of support, so it is particularly important for the structural optimization design of flexible hinge.

Taking the biaxial flexural mount in this article as an example, the short straight beam in the middle of the "L-shaped" flexible groove on the flexural mount is an important part of the flexible hinge, which allows the flexural mount to undergo certain deformation and displacement, so as to achieve the purpose of offloading the gravity load. The "L-shaped" hinge can be equivalent to a flexible sheet, as shown in Figure 17, the flexible sheet can allow movement of the sheet out of the plane. The critical dimensions: height h , width w , and thickness t of the short straight beam are optimized so that the flexible hinge will not be "over-flexible" or "over-rigid."

Firstly, the stiffness characteristics of the flexure hinge are analyzed. The compressive stiffness of the z direction of the flexure mount is shown in formula (5) (ZS, Wang 2019)

$$k_z = \frac{Etw}{h} \quad (5)$$

The stiffness along the y direction is shown in formula (6) (ZS, Wang 2019)

$$k_y = \frac{k_z t^2}{(1 - \mu^2)h^2 + 2.4(1 + \mu)t^2} = \frac{Et^3 w}{(1 - \mu^2)h^3 + 2.4(1 + \mu)t^2 h} \quad (6)$$

The rotational stiffness of direction z and direction x is shown in Formula (7) and (8) (ZS, Wang 2019)

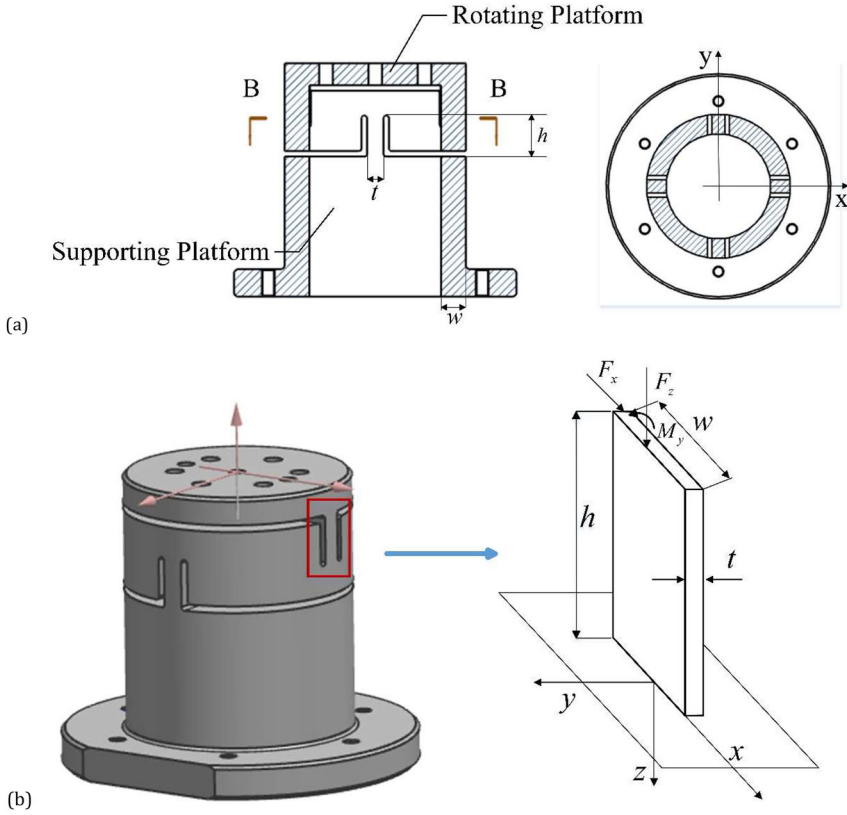


Figure 17. Flexural mount, (a) Cross-sectional view of the flexural mount, (b) stiffness analysis schematic diagram of short straight beam with flexural mount.

$$k_{\theta_x} = \frac{Et^3 w}{12h(1 - \mu^2)} \quad (7)$$

$$k_{\theta_z} = \frac{Et^3 w}{12} \left[\frac{1}{2(1 + \mu)} \left(4 + 2.52 \frac{t}{w} \right) + \frac{w^2}{(1 - \mu^2) + 2.4(1 + \mu)t^2} \right] \quad (8)$$

where E is the elastic modulus and μ is the material Poisson's ratio.

From the above analysis, for a single flexural mount, increasing the height h of the short straight beam or reducing the thickness t and width w of the short straight beam will reduce the overall stiffness of the flexural mount in its axial direction, allowing the flexible hinge certain deformation and displacement occur, offloading force load and thermal load. At the same time, in order to maintain the stiffness of the z -direction support, the width w must not be too low. To ensure that the short straight beam does not buckle, the ratio of the height h to the thickness t must not be too large, so the next step is to optimize the size $h/w/t$, analyze the influence of different structure size combinations on the RMS of the mirror. We established a flexure hinge model and optimize the three critical dimensions of the flexure hinge at the same time to obtain the critical dimensions to ensure the surface figure accuracy.

Figures 18 and 19 respectively show the relationship between the three critical dimensions of the flexure hinge and the surface accuracy and the first-order natural frequency in Four Dimension Space form visually. In the Figures 18 and 19, x -axis, y -axis and z -axis correspond to variables, and color is used to show the change of x -direction surface error, y -direction surface error, and fundamental frequency when the critical dimensions are different.

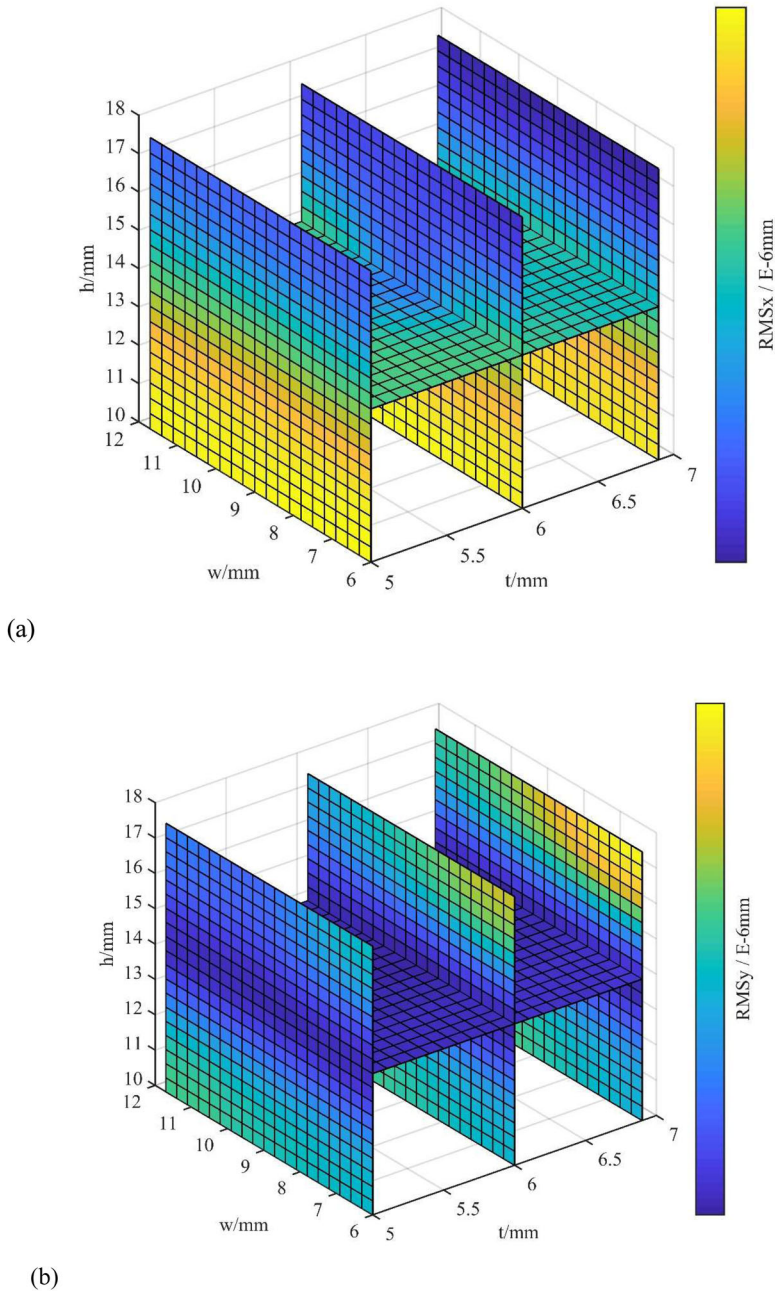


Figure 18. Effect of critical dimensions of flexure hinges on RMS. (a) Effect on x-direction RMS_x . (b) Effect on y-direction RMS_y .

As shown in Figure 18, the values of critical dimensions within the respective size ranges are different, and the mirror shape accuracy is different. The larger the h value is, the better the x-direction surface figure accuracy is, but it is not sensitive to the changes of the width w and the thickness t of the short straight beam. For the y-direction surface figure accuracy, the change of the width and the thickness of the short straight beam has almost no effect on the y-direction surface figure accuracy. If the height h of the short straight beam is too large or too small, the surface figure will deteriorate, so choose appropriate h value is particularly important to ensure

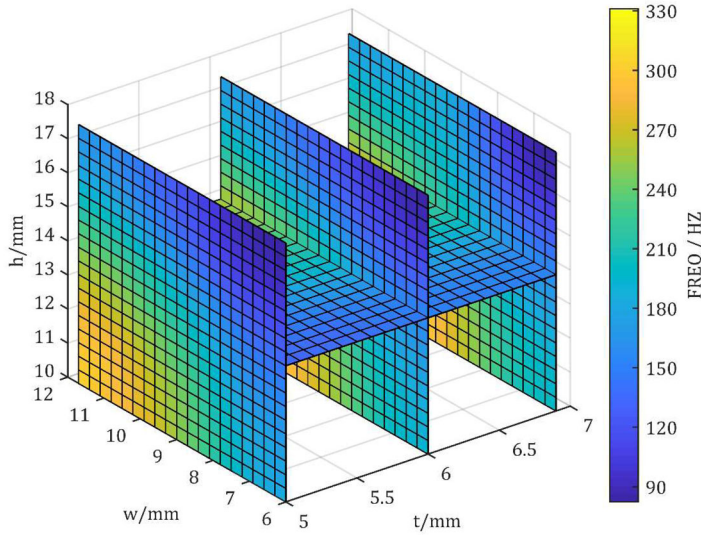


Figure 19. Effect of critical dimensions of flexure hinges on the fundamental frequency.

Table 3. Critical dimensions of flexural mount.

Item	Value/mm
Height of short straight beam h	14
Width of short straight beam w	9
Thickness of short straight beam t	6

the shape accuracy of the x/y direction. It can be seen that the “over-flexible” or “over-rigid” of the flexible hinge will lead to the deterioration of the shape accuracy of the mirror. The effect of the critical dimension $h/w/t$ of the flexible hinge on the natural frequency of the mirror assembly is shown in Figure 19. Increasing the width w of the short straight beam or the thickness t of the short straight beam will result in an increase in the fundamental frequency of the mirror assembly. The fundamental frequency is more sensitive to the change of the width w of the short straight beam, and with the increase of the height h of the short straight beam, the fundamental frequency of the mirror decreases. Combined with the analysis of the stiffness of the flexible hinge, increasing the value of w/t and reducing the value of h will cause the rigidity of the flexible hinge to increase, thereby improving the static and dynamic stiffness of the mirror assembly and increasing the fundamental frequency of the assembly.

Based on the analysis above, the critical dimensions of the flexural mount are finally determined as shown in Table 3. At this time, the accuracy of the mirror surface is $RMS_x=4.97$ nm, $RMS_y=2.91$ nm. The first-order natural frequency is 228.27HZ. Figures 20 and 21 shows the mirror deformation fringe after removing the rigid body displacement.

Sensitivity analysis was performed using the controlled variable method. Sensitivity was defined as the standard deviation of the dependent variable divided by the standard deviation of the independent variable. Each independent variable has a fixed value range, so its unit independent variable variance is fixed. Therefore, the greater the ratio of the standard deviation of the dependent variable to the standard deviation of the independent variable, the more sensitive it is to the independent variable. As shown in Figure 22, the x -direction surface shape accuracy is the most sensitive to t , and the y -direction surface shape accuracy is the most sensitive to h , which is consistent with the surface shape results obtained by the finite element analysis.

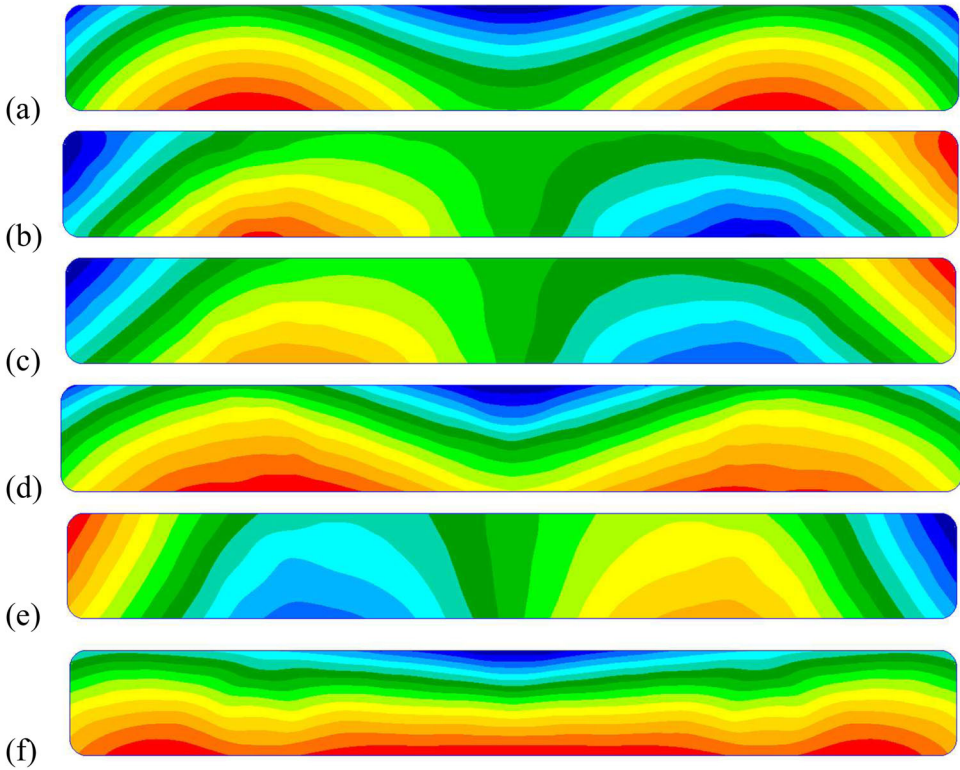


Figure 20. The modal shapes of the first 6 modes, (a) $F1 = 228.27$ Hz, (b) $F2 = 232.8$ Hz, (c) $F3 = 260.57$ Hz, (d) $F4 = 265.41$ Hz, (e) $F5 = 281.76$ Hz, (f) $F6 = 292.15$ Hz.

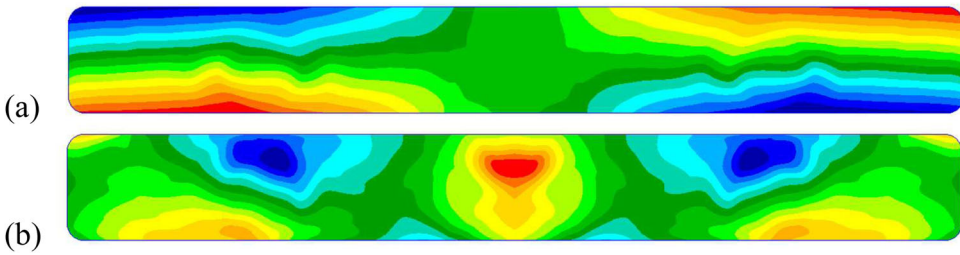


Figure 21. The deformation fringe of static analysis results, (a) surface distortion due to x-direction gravity, $RMS_x = 4.97$ nm, (b) surface distortion due to y-direction gravity, $RMS_y = 2.91$ nm.

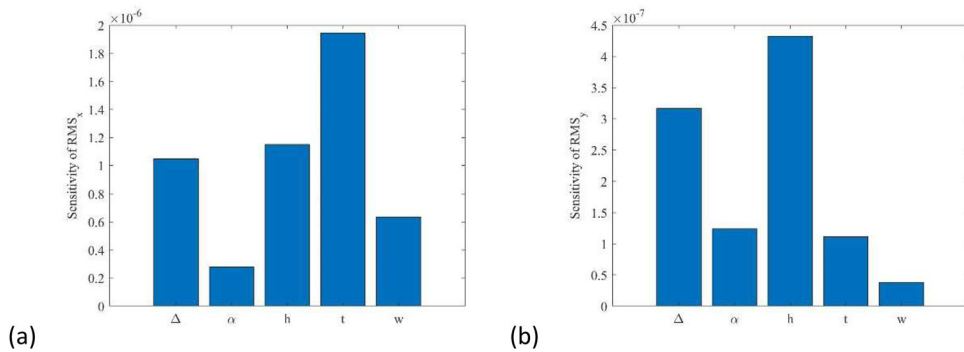


Figure 22. Sensitivity analysis of RMS on biaxial flexure with respect to the flexure dimension parameters, (a) Sensitivity analysis of RMS_x , (b) Sensitivity analysis of RMS_y .

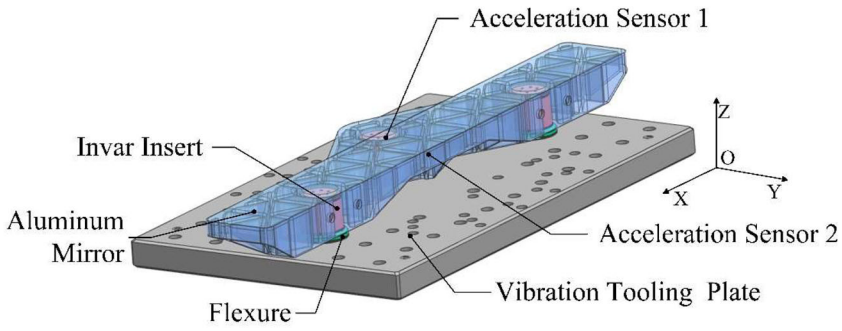


Figure 23. Prototype components.

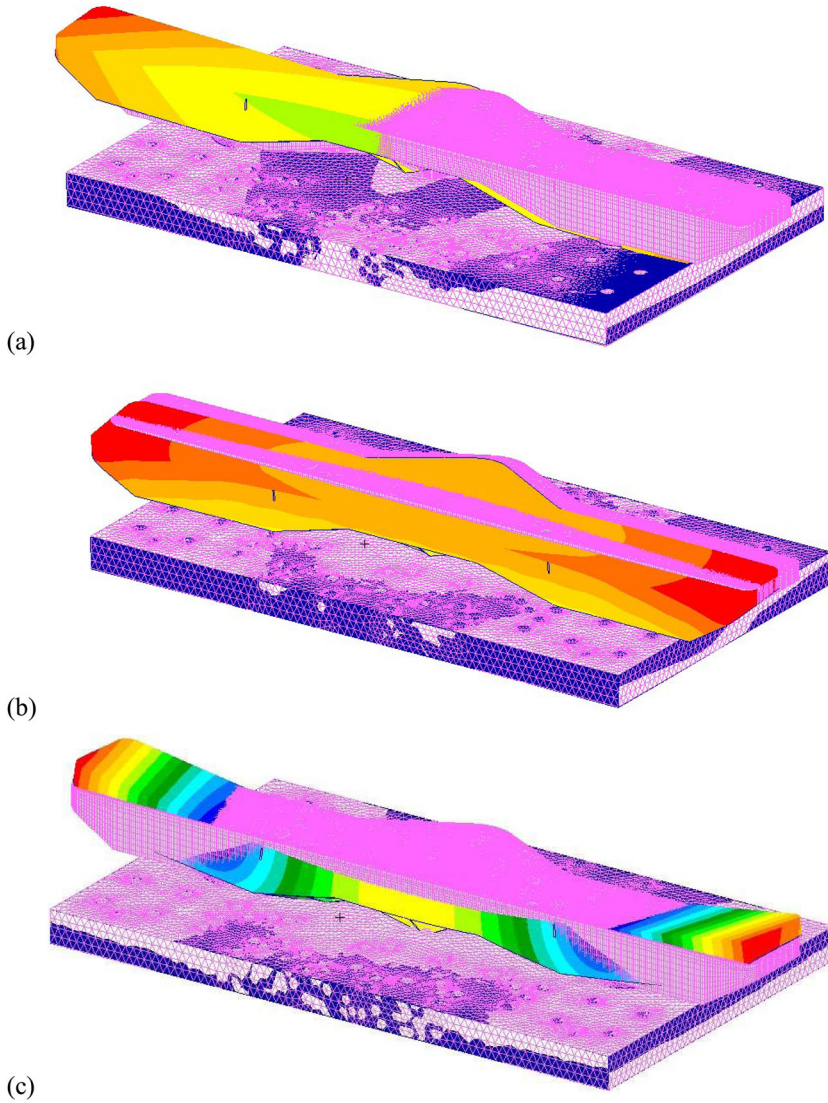


Figure 24. First order translational modes in x/y/z three directions of the prototype, (a) x-direction, (b) y-direction, (c) z-direction.



Figure 25. Vibration test of prototype.

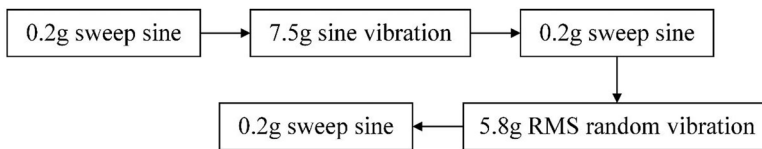


Figure 26. Vibration test of prototype process.

4. Vibration test

In order to verify the rationality of mirror component design and the accuracy of simulation analysis, eliminate unreasonable factors as early as possible in the early stage of design, and reduce the cost and shorten the development period, a simulation prototype of mirror is prepared for vibration test. In order to simulate the characteristics of the RB-SiC mirror as much as possible, the position of the gravity center and mass of the aluminum mirror are as same as those of the RB-SiC mirror, and the flexural mount and inserts of the mirror are manufactured according to the flight model, and then the dynamic vibration test is carried out on the force and heat sample simulation part of the mirror component. As shown in Figure 23, the vibration test assembly consists of an aluminum mirror, an invar insert, a titanium alloy flexural mount and an aluminum tooling support plate.

4.1. Modal analysis of simulated prototype

Before the vibration test of the simulated prototype is started, the finite element analysis of the prototype is required to verify the rationality of the vibration tooling design. The fringe of the modal shape of the assembly can be obtained, as shown in Figure 24, which are the first-order vibration shapes of the prototype component in three directions $x/y/z$.

4.2. Vibration test of prototype

The vibration test will be carried out in the environmental test station of the CIOMP. As shown in Figure 25, the test components are installed on the vibrating table, and the acceleration sensor

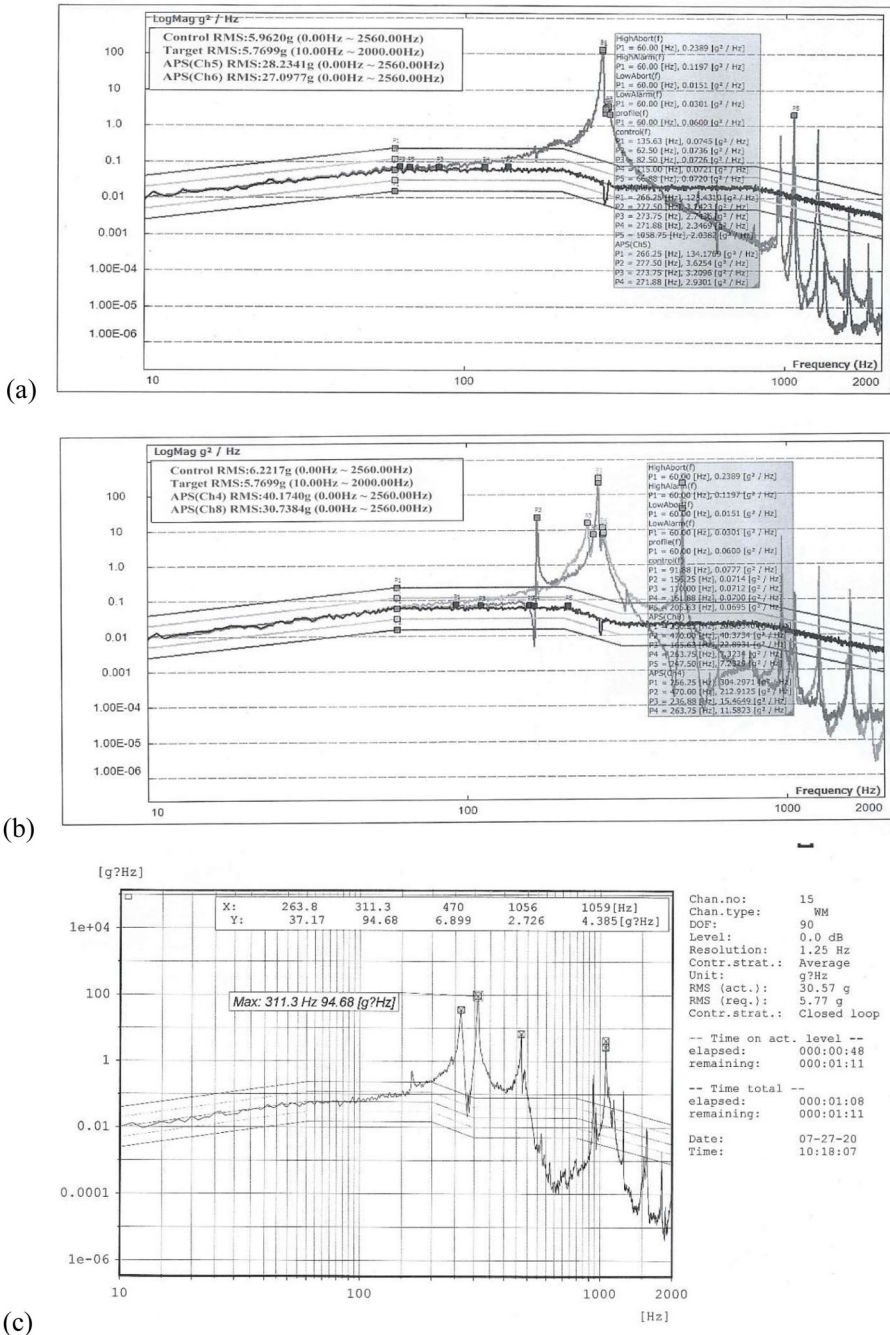


Figure 28. Random vibration test results of the mirror, (a) x-direction random vibration test, (b) y-direction random vibration test, (c) z-direction random vibration test.

the structural system. The reliability of the structure can be verified by random vibration test. The prototype vibration test process is shown in the Figure 26.

The fundamental frequency of the prototype was obtained by sine sweep test and the sine sweep test of the simulation prototype was carried out in the range of 10–2000 Hz. The fundamental frequency in x/y/z directions was analyzed respectively, as shown in Figure 27. The

Table 4. Comparative analysis of simulation results and test results.

	x-direction		y-direction		z-direction	
	fundamental frequency /HZ	relative errors	fundamental frequency /HZ	relative errors	fundamental frequency /HZ	relative errors
Simulation	274.211	0.95%	260.89	1.52%	186.31	8.96%
Test	276.85		264.93		166.4	

maximum test value of fundamental frequency of the prototype in the x-direction was 276.85 Hz, and the natural frequency value of simulation analysis was 274.21 Hz, the relative error is 0.95%. The maximum test value of the fundamental frequency of the prototype in the y-direction is 264.93 Hz, the fundamental frequency value of the simulation analysis is 260.89 Hz, the relative error is 1.52%. The maximum test value of the fundamental frequency of the prototype in the z-direction is 166.4 Hz, the natural frequency value of simulation analysis is 186.31 Hz, and the relative error between the two is 8.96%. The comparative analysis shows that the finite element analysis results of the simulated prototype are accurate, with high connection reliability and good dynamic stiffness in three directions.

Random vibration test to validate the reliability of the component structure, three directions on the random vibration acceleration response power spectral density curve as shown in [Figure 28](#), general three directions on the random vibration acceleration response power spectral density curve, components in three directions acceleration response of the first-order near the resonance frequency is not large, the structure of the dynamic performance is good.

5. Conclusions

In this paper, the structure design of the large aspect ratio rectangular mirror and a novel biaxial flexural mount is carried out, and the simulation optimization analysis is carried out for the biaxial flexural mount. The optimal design of the biaxial flexural mount can meet the requirements of ensuring the large aspect ratio mirror shape accuracy and increasing the fundamental frequency of the mirror assembly. The slim light-weighted space-borne mirror has a very large aspect ratio. Under the action of 1 G gravity, the x-direction/y-direction surface accuracy is $RMS_x = 4.97$ nm, $RMS_y = 2.91$ nm and the fundamental frequency is 228.27 Hz. [Table 4](#) shows the comparison between the simulation results and the experimental results.

The flexural mount technology proposed in this article can be applied to any reflective optics that takes the form of back mount and has a higher demand for surface accuracy. The optimization method proposed in this article is also applicable to other similar forms of flexural mount to optimize the structure and improve the mirror surface accuracy of the mirror.

Acknowledgements

Thanks are due to the reviewers for the revised comments. The first author would like to thank her teacher for his help with the research work.

Disclosure statement

The authors declare that there are no conflicts of interest related to this article.

Funding

This work is supported by Jilin Provincial Scientific and Technological Development Program, China (Grant Nos. 20180201015GX and 20180414066GH)

ORCID

Zongxuan Li  <http://orcid.org/0000-0001-5239-6789>

References

- Arijit, D. H., K. P. Chetan, K. Subrata, T. Umut, and D. Tayfun. 2018. Prediction and analysis of optimal frequency of layered composite structure using higher-order FEM and soft computing techniques. *Steel and Composite Structures* 29 (6):749.
- Bhattacharya, S., G. K. Anantha Suresh, and A. Ghosal. 2018. Design of a one-dimensional flexible structure for desired load-bearing capability and axial displacement. *Mechanics Based Design of Structures and Machines* 46 (3):376–99. doi:10.1080/15397734.2018.1439755.
- Doyle, K. B., V. L. Genberg, and G. L. Michels. 2012. *Integrated Optomechanical Analysis*. Trans. H. D. Lian, X.Y. Wang, and P. Xu. 2nd. ed. Beijing: National Defense Industry Press.
- Figoski, J. W. 1999. The quickbird telescope: The reality of large, high-quality, commercial space optics. *SPIE* 3779: 22–30. doi:10.1117/12.368209.
- Guo, J., L. Zhu, J. Zhao, and D.-P. Gong. 2019. Design and optimize of high tolerance support structure for large aperture space mirror. *Optics and Precision Engineering* 27 (5):1138–47.
- Kihm, H., H. S. Yang, K. Moon, J. H. Yeon, S. H. Lee, and Y. W. Lee. 2012. Adjustable bipod flexures for mounting mirrors in a space telescope. *Applied Optics* 51 (32):7776–83. doi:10.1364/AO.51.007776.
- Lalepalli, A. P., K. S. Subrata, H. Nitin, K. Chetan, and T. Umut. 2020. Optimal fiber volume fraction prediction of layered composite using frequency constraints—A hybrid FEM approach. *Computers and Concrete* 25:303–10.
- Li, H. X., Y. L. Ding, and H. W. Zhang. 2015. Support system study of rectangular mirror. *Acta Optica Sinica* 35 (5):337–44.
- Li, Z. X., X. Chen, and G. Jin. 2018. Dimensionless design model for biaxial cartwheel flexure hinges. *Mechanics Based Design of Structures and Machines* 46 (4):401–9. doi:10.1080/15397734.2017.1341841.
- Li, Z. X., X. Chen, S. J. Wang, and G. Jin. 2017. Optimal design of a $\Phi 760$ mm lightweight Sic mirror and the flexural mount for a space telescope. *Review of Scientific Instruments* 88 (12):125107–25. doi:10.1063/1.4986042.
- Liu, B., W. Wang, Y. J. Qu, X. P. Li, X. Wang, and H. Zhao. 2018. Design of an adjustable bipod flexure for a large-aperture mirror of a space camera. *Applied Optics* 57 (15):4048–55. doi:10.1364/AO.57.004048.
- Omid, M., D. S. Fathollahi, and K. M. Habibnejad. 2020. Dynamic modelling and extended bifurcation analysis of flexible-link manipulator. *Mechanics Based Design of Structures and Machines* 48 (1):87–110.
- Riabtsev, M., V. Petuya, M. Urizar, and E. Macho. 2020. Design and analysis of an active 2-DOF lockable joint. *Mechanics Based Design of Structures and Machines*. doi:10.1080/15397734.2020.1784203.
- Suzuki, S., Y. Kankaku, H. Imai, and Y. Osawa. 2012. Overview of ALOS-2 and ALOS-3. *SPIE* 8528:852811.
- Wang, Z. S. 2019. Research on structure optimization of large aperture monolithic space-based mirror and its mounting technology. PhD diss., Changchun Institute of Optics, Fine Mechanics and Physics, Chinese Academy of Science, China.
- Zhang, Z., X. S. Quan, H. Wang, T. Y. Liu, Z. Xiong, X. D. Yuan, and Y. M. Rong. 2017. Optomechanical analysis of the flexure mounting configuration of large aperture laser transport mirror. *Optical Engineering* 56 (2): 025103. doi:10.1117/1.OE.56.2.025103.